

Non-Parametric Neuro-Adaptive Coordination of Multi-Agent Systems

Christos K. Verginis
 University of Texas at Austin
 Texas, USA
 cverginis@utexas.edu

Zhe Xu
 Arizona State University
 Arizona, USA
 xzhe1@asu.edu

Ufuk Topcu
 University of Texas at Austin
 Texas, USA
 utopcu@utexas.edu

ABSTRACT

We develop a learning-based algorithm for the distributed formation control of networked multi-agent systems governed by unknown, nonlinear dynamics. Most existing algorithms either assume certain parametric forms for the unknown dynamic terms or resort to unnecessarily large control inputs in order to provide theoretical guarantees. The proposed algorithm avoids these drawbacks by integrating neural network-based learning with adaptive control in a two-step procedure. In the first step of the algorithm, each agent learns a controller, represented as a neural network, using training data that correspond to a collection of formation tasks and agent parameters. These parameters and tasks are derived by varying the nominal agent parameters and the formation specifications of the task in hand, respectively. In the second step of the algorithm, each agent incorporates the trained neural network into an online and adaptive control policy in such a way that the behavior of the multi-agent closed-loop system satisfies a user-defined formation task. Both the learning phase and the adaptive control policy are distributed, in the sense that each agent computes its own actions using only local information from its neighboring agents. The proposed algorithm does not use any *a priori* information on the agents' unknown dynamic terms or any approximation schemes. We provide formal theoretical guarantees on the achievement of the formation task.

KEYWORDS

Multi-Agent Systems, Adaptive Control, Neural Networks, Machine Learning

1 INTRODUCTION

During the last decades, decentralized control of networked multi-agent systems has attracted significant attention due to the great variety of its applications, including multi-robot systems, transportation, multi-point surveillance as well as biological systems [5, 18, 26]. In such systems, each agent calculates its own actions based on local information, as modeled by a connectivity graph, without relying on any central control unit. This absence of central

control and global information motivates leader-follower architectures, where a team of agents (followers) aims at following a pre-assigned leader agent that holds information about the execution of a potential task. The coordination problem of leader-follower architectures has been the focus of many works [2, 16, 24, 25, 33, 39] because of its numerous applications in various disciplines including autonomous vehicles coordination (satellite formation flying, cooperative search of unmanned aerial vehicles and synchronization of Euler–Lagrange systems), systems biology (control and synchronization in cellular networks), and power systems (control of renewable energy microgrids).

Although many works on distributed cooperative control consider known and simple dynamic models, there exist many practical engineering systems that cannot be modeled accurately and are affected by unknown exogenous disturbances. Thus, the design of control algorithms that are robust and adaptable to such uncertainties and disturbances is important. For multi-agent systems, ensuring robustness is particularly challenging due to the lack of global information and the interacting dynamics of the individual agents. A promising step towards the control of systems with uncertain dynamics is the use of data obtained *a priori* from system runs. However, engineering systems often undergo purposeful modifications (e.g., substitution of a motor or link in a robotic arm or exposure to new working environments) or suffer gradual faults (e.g., mechanical degradation), which might change the systems' dynamics or operating conditions. Therefore, one cannot rely on the aforementioned data to provably guarantee the successful control of the system. On the other hand, the exact incorporation of these changes in the dynamic model, and consequently, the design of new model-based algorithms, can be a challenging and often impossible procedure. Hence, the goal in such cases is to exploit the data obtained *a priori* and construct intelligent online policies that achieve a user-defined task while adapting to the aforementioned changes.

1.1 Contributions

This paper addresses the distributed coordination of networked multi-agent systems governed by unknown nonlinear dynamics. Our main contribution lies in the development of a distributed learning-based control algorithm that provably *guarantees* the accomplishment of a given multi-agent formation task without any *a priori* information on the underlying dynamics. The algorithm draws a novel connection between distributed learning with neural-network-based representations and adaptive feedback control, and consists of the following steps. Firstly, it trains a number of neural networks, one for each agent, to approximate controllers for the agents that accomplish the given formation task. The data used to

Permission to make digital or hard copies of all or part of this work for personal or classroom use is granted without fee provided that copies are not made or distributed for profit or commercial advantage and that copies bear this notice and the full citation on the first page. Copyrights for components of this work owned by others than ACM must be honored. Abstracting with credit is permitted. To copy otherwise, or republish, to post on servers or to redistribute to lists, requires prior specific permission and/or a fee. Request permissions from permissions@acm.org.

ACM Conference, July 2017, Washington, DC, USA. © 2022 Association for Computing Machinery.

train the neural networks consist of pairs of states and control actions of the agents that are gathered from runs of the multi-agent system. Secondly, it uses an online adaptive feedback control policy that guarantees accomplishment of the given formation task. Both steps can be executed in a distributed manner in a sense that each agent uses only local information, as modeled by a connectivity graph. Our approach builds on a combination of controllers trained off-line and on-line adaptations, which was recently shown to significantly enhance performance with respect to single use of the off-line part [3]. Numerical experiments show the robustness and adaptability of the proposed algorithm to different formation tasks, interactions among the agents, and system dynamics. That is, the proposed algorithm is able to achieve the given formation task even when the neural networks are trained with data that correspond to different multi-agent dynamic models (resembling a change in the dynamics of the agents), as well as different formation tasks and interactions among the agents.

1.2 Related Work

Robust and adaptive control: A large class of works on multi-agent coordination considers neuro-adaptive control with stability guarantees, focusing also on optimal control [9, 16, 17, 21–25, 30, 31, 33, 38, 39]. Nevertheless, drawing motivation from the neural-network density property (see, e.g., [6]), these works base their theoretical results on the property that the unknown terms (dynamic, optimal controllers, or value functions) can be approximated accurately by single-layer, linearly parameterized neural networks. Similarly, traditional adaptive-control techniques assume that the structure of the system dynamics is known and that the unknown terms are linearly parameterized with respect to unknown but constant parameters [4, 37]. On the contrary, we relax these assumptions and propose a non-parametric neuro-adaptive distributed multi-agent control policy, whose stability guarantees rely on a mild boundedness condition on the state of the closed-loop system that is driven by the learned controller.

Multi-agent coordination with unknown nonlinear continuous dynamics has been also tackled in the literature by using the so-called funnel control, without using dynamic approximations [1, 2, 32, 34]. Nevertheless, funnel controllers depend on so-called reciprocal time-varying barrier functions that drive the control input unbounded when the error approaches a pre-specified funnel, creating thus unnecessarily large control inputs that cannot be realized by the system's actuators.

Reinforcement learning of stochastic systems: Another class of related works tackling multi-agent coordination with unknown dynamics is the area of cooperative reinforcement learning with stochastic processes [7, 8, 11–15, 19, 27, 35, 36, 40–42]. However, such works usually adopt the conservative assumption that the agents have access to the states and actions of all other agents in the learning, execution, or both phases [11–14]. Moreover, these works exhibit scalability problems with respect to the number of agents [15], or assume the availability of time or state discretizations of the underlying continuous-time and continuous-state models. Additionally, the related works on multi-agent cooperative reinforcement learning usually consider common or team-average reward functions for the agents [7, 41, 42], which cannot be easily

extended to account for inter-agent formation specifications that we account for. When relative inter-agent formation specifications are considered, the environment becomes non-stationary creating problems in the theoretical convergence analysis [42].

2 PROBLEM FORMULATION AND PRELIMINARIES

Consider a networked multi-agent group comprised of a leader, indexed by $i = 0$, and N followers, with $\mathcal{N} := \{1, \dots, N\}$. The leading agent acts as an ecosystem that generates a desired command/reference trajectory for the multi-agent group. The followers, which have to be controlled, evolve according to the 2nd-order dynamics

$$\dot{x}_{i,1}(t) = x_{i,2}(t) \quad (1a)$$

$$\dot{x}_{i,2}(t) = f_i(x_i(t), t) + g_i(x_i(t), t)u_i(t) \quad (1b)$$

where $x_i := [x_{i,1}^\top, x_{i,2}^\top]^\top \in \mathbb{R}^{2n}$ is the i th agent's state, assumed available for measurement by agent i , $f_i : \mathbb{R}^{2n} \times [0, \infty) \rightarrow \mathbb{R}^n$, $g_i : \mathbb{R}^{2n} \times [0, \infty) \rightarrow \mathbb{R}^n$ are unknown functions modeling the agent's dynamics, and u_i is the i th agent's control input. The vector fields $f_i(\cdot)$ and $g_i(\cdot)$ are assumed to be locally Lipschitz in x_i over \mathbb{R}^{2n} for each fixed $t \geq 0$, and uniformly bounded in t over $[t_0, \infty)$ for each fixed $x_i \in \mathbb{R}^{2n}$, for all $i \in \mathcal{N}$. The dynamics (1) comprise a large class of nonlinear dynamical systems that capture contemporary engineering problems in mechanical, electromechanical and power electronics applications, such as rigid/flexible robots, induction motors and DC-to-DC converters, to name a few. The continuity in time and state provides a direct link to the actual underlying systems, and we further do not require any time or state discretizations. Moreover, the 2nd-order model (1) can be easily extended to account for higher-order integrator systems [29].

We do not assume any knowledge of the structure, Lipschitz constants, or bounds of $f_i(\cdot)$ and $g_i(\cdot)$, and we do not use any scheme to approximate them. Nevertheless, we do require the following assumption on $g_i(\cdot)$:

ASSUMPTION 1. *The matrices $g_i(x_i, t)$ are positive definite, for all $(x_i, t) \in \mathbb{R}^{2n} \times [0, \infty)$.*

Assumption 1 is a sufficiently controllability condition for (1); intuitively, it states that the multiplier of u (the input matrix) do not change the direction imposed to the system and is adopted in the majority of the related works (e.g., [2, 17, 32, 38]). Systems not covered by (1) or Assumption 1 consist of underactuated or non-holonomic systems, such as unicycle robots, underactuated aerial or underwater vehicles. Such systems require special attention and consist part of our future work.

We use an undirected graph $\mathcal{G} := (\mathcal{N}, \mathcal{E})$ to model the communication among the agents, with \mathcal{N} being the index set of the agents, and $\mathcal{E} \subseteq \mathcal{N} \times \mathcal{N}$ being the respective edge set, with $(i, i) \notin \mathcal{E}$ (i.e., simple graph). The adjacency matrix associated with the graph \mathcal{G} is denoted by $\mathcal{A} := [a_{ij}] \in \mathbb{R}^{N \times N}$, with $a_{ij} \in \{0, 1\}$, $i, j \in \{1, \dots, N\}$. If $a_{ij} = 1$, then agent i obtains information regarding the state x_j of agent j (i.e., $(i, j) \in \mathcal{E}$), whereas if $a_{ij} = 0$ then there is no state-information flow from agent j to agent i (i.e., $(i, j) \notin \mathcal{E}$). Furthermore, the set of neighbors of agent i is denoted by $\mathcal{N}_i := \{j \in \mathcal{N} : (i, j) \in \mathcal{E}\}$, and the degree matrix is defined as

$\mathcal{D} := \text{diag}\{|\mathcal{N}_1|, \dots, |\mathcal{N}_N|\}$. Since the graph is undirected, the adjacency is a mutual relation, i.e., $a_{ij} = a_{ji}$, rendering \mathcal{A} symmetric. The *Laplacian* matrix of the graph is defined as $\mathcal{L} := \mathcal{D} - \mathcal{A}$ and is also symmetric. The graph is *connected* if there exists a path between any two agents. For a connected graph, it holds that $\mathcal{L}\bar{1} = 0$, where $\bar{1}$ is the vector of ones of appropriate dimension.

The state/command variables of the leading agent (indexed by 0) are denoted by $x_{0,1}, x_{0,2} \in \mathbb{R}^n$ and obey the 2nd-order dynamics

$$\begin{aligned}\dot{x}_{0,1}(t) &= x_{0,2}(t) \\ \dot{x}_{0,2}(t) &= u_0(t)\end{aligned}$$

for a smooth and bounded $u_0 : [0, \infty) \rightarrow \mathbb{R}^n$. However, the state of the leader is only provided to a subgroup of the N agents. In particular, the access of the follower agents to the leader's state is modeled by a diagonal matrix $\mathcal{B} := \text{diag}\{b_1, \dots, b_N\} \in \mathbb{R}^{N \times N}$; if $b_i = 1$, then the i th agent has access to the leader's state, whereas it does not if $b_i = 0$, for $i \in \mathcal{N}$. Thus, we may also define the augmented graph as $\bar{\mathcal{G}} := (\mathcal{N} \cup \{0\}, \bar{\mathcal{E}})$, where $\bar{\mathcal{E}} := \mathcal{E} \cup \{(i, 0) : b_i = 1\}$. We also define $\bar{x}_1 := [x_{1,1}^\top, \dots, x_{N,1}^\top]^\top \in \mathbb{R}^{Nn}$, $\bar{x}_2 := [x_{1,2}^\top, \dots, x_{N,2}^\top]^\top \in \mathbb{R}^{Nn}$, $\bar{x} := [\bar{x}_1^\top, \dots, \bar{x}_N^\top]^\top \in \mathbb{R}^{2Nn}$ and $\bar{x}_{0,1} := [x_{0,1}^\top, \dots, x_{0,1}^\top]^\top \in \mathbb{R}^{Nn}$, $\bar{x}_{0,2} := [x_{0,2}^\top, \dots, x_{0,2}^\top]^\top \in \mathbb{R}^{Nn}$, $\bar{x}_0 := [\bar{x}_{0,1}^\top, \bar{x}_{0,2}^\top]^\top \in \mathbb{R}^{2Nn}$. By further defining $\bar{f}(\bar{x}, t) := [f_1(x_1, t)^\top, \dots, f_N(x_N, t)^\top]^\top \in \mathbb{R}^{Nn}$, $\bar{g}(\bar{x}, t) := \text{diag}\{g_1(x_1, t), \dots, g_N(x_N, t)\} \in \mathbb{R}^{Nn \times Nn}$, $\bar{u}(t) := [u_1(t)^\top, \dots, u_N(t)^\top]^\top \in \mathbb{R}^{Nn}$, (1) can be written as

$$\dot{\bar{x}}_1(t) = \bar{x}_2(t) \quad (2a)$$

$$\dot{\bar{x}}_2(t) = \bar{f}(\bar{x}(t), t) + \bar{g}(\bar{x}(t), t)\bar{u}(t) \quad (2b)$$

The goal of this work is to design a distributed control algorithm, where each agent has access only to its neighbors' information, to achieve a pre-specified geometric formation of the agents in \mathbb{R}^n . More specifically, consider for each agent $i \in \mathcal{N}$ the constants c_{ij} , $j \in \{0\} \cup \mathcal{N}_i$ prescribing a desired offset that agent i desires to achieve with respect to the leader ($j = 0$), and its neighbors ($j \in \mathcal{N}_i$). That is, each agent $i \in \mathcal{N}_i$ aims at achieving $x_{i,1} = x_{j,1} - c_{ij}$, for all $j \in \mathcal{N}_i$, and if $b_i = 1$ (i.e., the agent is connected to the leader), $x_{i,1} = x_{0,1} - c_{i0}$. Note that $c_{ij} = -c_{ji}$, for all $i, j \in \mathcal{E}$, and we assume that the set

$$\begin{aligned}\{\bar{x}_1 \in \mathbb{R}^{Nn} : x_{i,1} - x_{j,1} + c_{ij} = 0, \forall (i, j) \in \mathcal{E}, \\ b_i(x_{i,1} - x_{0,1} + c_{i0}) = 0, \forall i \in \mathcal{N}\}\end{aligned}$$

is non-empty in order for the formation specification to be feasible. Furthermore, we impose the following assumption on the graph connectivity:

ASSUMPTION 2. *The graph \mathcal{G} is connected and there exists at least one $i \in \mathcal{N}$ such that $b_i = 1$.*

The aforementioned assumption dictates that $\mathcal{L} + \mathcal{B}$ is an irreducibly diagonally dominant M-matrix [15]. An M-matrix is a square matrix having its off-diagonal entries non-positive and all principal minors nonnegative, thus $\mathcal{L} + \mathcal{B}$ is positive definite [15].

We define now the error variables for each agent as

$$e_{i,1} := \sum_{j \in \mathcal{N}_i} (x_{i,1} - x_{j,1} + c_{ij}) + b_i(x_{i,1} - x_{0,1} + c_{i0}) \quad (3)$$

for $i \in \mathcal{N}$. By defining $\bar{e}_1 := [e_{1,1}^\top, \dots, e_{N,1}^\top]^\top$, employing the multi-agent graph properties and noticing that $(\mathcal{L} \otimes I_n)\bar{x}_{0,1} = 0$, where

\otimes denotes the Kronecker product, (3) can be written as

$$\bar{e}_1 := H(\bar{x}_1 - \bar{x}_{0,1} + \bar{c}), \quad (4)$$

where $H := (\mathcal{L} + \mathcal{B}) \otimes I_n$, and

$$\bar{c} := \begin{bmatrix} c_1 \\ \vdots \\ c_N \end{bmatrix} := ((\mathcal{L} + \mathcal{B}) \otimes I_n)^{-1} \begin{bmatrix} \sum_{j \in \mathcal{N}_1} c_{1j} + b_1 c_{10} \\ \vdots \\ \sum_{j \in \mathcal{N}_N} c_{Nj} + b_N c_{N0} \end{bmatrix} \quad (5)$$

stacks the relative desired offsets c_i of the i th agent with respect to the leader, as dictated by the desired formation specification. In this way, the desired formation is expressed with respect to the leader state, and is thus achieved when the state $x_{i,1}$ of each agent approaches the leader state $x_{0,1}$ with the corresponding offset c_i , $i \in \mathcal{N}$. Therefore, the formation control problem is solved if the control algorithm drives the disagreement vector

$$\bar{\delta}_1 := \begin{bmatrix} \delta_{1,1} \\ \vdots \\ \delta_{N,1} \end{bmatrix} := \bar{x}_1 - \bar{x}_{0,1} + \bar{c} \quad (6)$$

to zero. However, the disagreement formation variables $\delta_{i,1}$ are global quantities and thus cannot be measured distributively by each agent based on the local measurements, as they involve information directly from the leader as well as from the whole graph topology via employing the inverse of $\mathcal{L} + \mathcal{B}$ in (5). Nevertheless, from (4), the positive definiteness of $\mathcal{L} + \mathcal{B}$ implies

$$\|\bar{\delta}_1\| \leq \frac{\|\bar{e}_1\|}{\sigma_{\min}(H)} \quad (7)$$

where $\sigma_{\min}(\cdot)$ denotes the minimum singular value. Therefore, convergence of \bar{e}_1 to zero, which we aim to guarantee, implies convergence of $\bar{\delta}_1$ to zero. Before proceeding, we define the tuple $\mathcal{F} := (x_0, \bar{f}, \bar{g}, \bar{c}, \bar{\mathcal{G}}, \bar{x}(0))$ as the "formation instance", characterized by the leader profile, the agent dynamics, the desired formation offsets, the graph topology, and the initial conditions of the agents.

3 THEORETICAL RESULTS

This section describes the proposed algorithm, which consists of two steps. The first step consists of off-line learning of distributed controllers, represented as neural networks, using training data derived from runs of the multi-agent system. In the second step, we design an adaptive feedback control policy that uses the neural networks and provably guarantees achievement of the formation specification.

3.1 Neural-network learning

We assume the existence of data gathered from a finite set of T trajectories \mathcal{J} generated by a priori runs of the multi-agent system. More specifically, we consider that \mathcal{J} is decomposed as $\mathcal{J} = (\mathcal{J}_1, \dots, \mathcal{J}_N)$, where \mathcal{J}_i is the set of trajectories of agent $i \in \mathcal{N}$. Since the proposed control scheme is distributed, we consider that each agent i has access to the data from its own set of trajectories \mathcal{J}_i , which comprises the finite set

$$\mathcal{J}_i = \left\{ \bar{x}_i^k(t), \{\bar{x}_i^j\}_{j \in \mathcal{N}_i^k}, u_i^k \left(\bar{x}_i^k(t), \{\bar{x}_i^j\}_{j \in \mathcal{N}_i^k}, t \right) \right\}_{t \in \mathbb{T}_i}$$

where \mathbb{T}_i is a finite set of time instants, $\bar{x}_i^k \in \mathbb{R}^{2n}$ is the state trajectory of agent i for trajectory k , \mathcal{N}_i^k are the neighbors of agent

i in trajectory k , with $\{\bar{x}^j\}_{j \in \mathcal{N}_i^k}$ being their respective state trajectories (which agent i has access to, being their neighbor), and $u_i^k(\bar{x}_i^k(t), \{\bar{x}^j\}_{j \in \mathcal{N}_i^k}, t) \in \mathbb{R}^n$ is the control input trajectory of agent i , which is a function of time and of its own and its neighbors' states. Note that the agents' state trajectories and control input are compliant with the dynamics (1).

Each agent $i \in \mathcal{N}$ uses the data to train a neural network in order to approximate a controller that accomplishes the formation task. More specifically, each agent uses the tuples $\{\bar{x}_i^k(t), \{\bar{x}^j\}_{j \in \mathcal{N}_i^k}\}_{t \in \mathbb{T}_i}$ as input to a neural network, and $u_i^k(\bar{x}_i^k(t), \{\bar{x}^j\}_{j \in \mathcal{N}_i^k}, t)_{t \in \mathbb{T}_i}$ as the respective output targets, for all T trajectories. For the inputs corresponding to agents that are not neighbors of agent i in a trajectory k , we disable the respective neurons. For a given $\bar{x} \in \mathbb{R}^{2n}$, we denote by $u_{i,nn}(\bar{x})$ the output of the neural network of agent $i \in \mathcal{N}$, and $\bar{u}_{nn}(\bar{x}) := [u_{1,nn}(\bar{x})^\top, \dots, u_{N,nn}(\bar{x})^\top]^\top$.

We stress that we do not require the training trajectories \mathcal{J} to correspond to the formation instance \mathcal{F} specified in the problem formulation of Section 2. That is, each trajectory k might be derived from the execution of a formation instance $\mathcal{F}_k = (\bar{x}_0^k, \bar{f}^k, \bar{g}^k, \bar{c}^k, \bar{\mathcal{G}}^k, \bar{x}^k(0))$ that is different than \mathcal{F} specified in Section 2, i.e., different leader profile x_0^k , agent dynamics \bar{f}^k, \bar{g}^k , formation offsets \bar{c}^k , communication graph $\bar{\mathcal{G}}^k$, and initial agent conditions $\bar{x}^k(0)$. As shown in the experiments of Section 4, the proposed algorithm, consisting of the trained neural networks and the adaptive feedback control policy (illustrated in the next section), is still able to guarantee the accomplishment of the given formation task, as specified by the formation instance \mathcal{F} . This is an important attribute of the proposed scheme, since it illustrates its robustness and adaptability to different agent dynamics, formation tasks, and inter-agent communication topologies between the training data and the online execution.

3.2 Distributed Control Policy

We now design a distributed, adaptive feedback control policy to accomplish the formation task dictated by the graph topology $\bar{\mathcal{G}}$, the leader profile $x_0(t)$, and offsets \bar{c} given in Section 2. We first impose a minor assumption on the closed-loop system trajectories that are driven by the neural networks' outputs.

ASSUMPTION 3. *The stacked vector of outputs $\bar{u}_{nn}(\bar{x})$ of the trained neural networks satisfies*

$$\|H(\bar{f}(\bar{x}, t) + \bar{g}(\bar{x}, t)\bar{u}_{nn}(\bar{x}))\| \leq w_0\|\bar{x}_0\| + w\|\bar{x}\| + W \quad (8)$$

for positive constants w_0, w, W , for all $\bar{x} \in \mathbb{R}^{2Nn}$, $t \geq 0$.

Intuitively, Assumption 3 states that the neural-network outputs $u_{i,nn}(\cdot)$ are able to maintain the boundedness of the relative inter-agent dynamics by the leader's and agents' states as well as the constants w_0, w, W , which are considered to be *unknown*. The assumption is motivated by the property of neural networks to approximate a continuous function arbitrarily well in a compact domain for a large enough number of neurons and layers [6]. Contrary to the related works (e.g., [9, 17, 21, 22, 24, 30]), however, we do not adopt approximation schemes for the system dynamics

and we do not impose restrictions on the size of w_0, w, W . Moreover, Assumption 3 does not imply that the neural-network outputs $u_{i,nn}(\bar{x}, t)$ guarantee accomplishment of the formation task. Instead, it is merely a growth condition.

We now design the adaptive feedback control policy. Consider the adaptation variables $\hat{d}_{i,1}, \hat{d}_{i,2}$ for each agent $i \in \mathcal{N}$, corresponding to upper bounds of w_0, w , and W in (8). Consider the augmented errors for each agent

$$e_{i,2} := \dot{e}_{i,1} + k_{i,1}e_{i,1} \quad (9)$$

where $k_{i,1}$ are positive constants, for all $i \in \mathcal{N}$. We design the distributed control policy as

$$u_i(\bar{x}, \hat{d}_{i,1}, \hat{d}_{i,2}) = u_{i,nn}(\bar{x}) - (k_{i,2} + \hat{d}_{i,1})e_{i,2} - \hat{d}_{i,2}\hat{e}_{i,2} \quad (10a)$$

where $k_{i,2}$ are positive constants, and $\hat{e}_{i,2}$ are defined as $\hat{e}_{i,2} := \frac{e_{i,2}}{\|e_{i,2}\|}$ if $e_{i,2} \neq 0$ and $\hat{e}_{i,2} := 0$ otherwise, for all $i \in \mathcal{N}$. The adaptation variables $\hat{d}_{i,1}, \hat{d}_{i,2}$ are updated as

$$\dot{\hat{d}}_{i,1} := \mu_{i,1}\|e_{i,2}\|^2 \quad (10b)$$

$$\dot{\hat{d}}_{i,2} := \mu_{i,2}\|e_{i,2}\| \quad (10c)$$

where $\mu_{i,1}, \mu_{i,2}$ are positive constants, for all $i \in \mathcal{N}$.

REMARK 1. *The control design is inspired by adaptive control methodologies [20], where the time-varying coefficients $\hat{d}_{i,1}, \hat{d}_{i,2}$ adapt to the unknown dynamics and counteract the effect of w_0, w , and W in (8) in order to ensure closed-loop stability. Note that agent i 's control policy (10) does not use any information on its own or its neighbors' dynamic terms $f_i(\cdot), g_i(\cdot)$, or the constants w_0, w , and W . Additionally, note that each agent uses only relative feedback from its neighbors, as can be verified by (3), (9) and (10).*

The accomplishment of the task is guaranteed by the following theorem, whose proof is given in Appendix A.

THEOREM 1. *Let a multi-agent system evolve subject to the dynamics (1), aiming to achieve a formation task dictated by the constants c_{ij} , $(i, j) \in \bar{\mathcal{E}}$. Under Assumptions 1, 3, the distributed control mechanism guarantees $\lim_{t \rightarrow \infty}(e_{i,1}, e_{i,2}) = 0$, for all $i \in \mathcal{N}$, as well as the boundedness of all closed-loop signals.*

Contrary to the works in the related literature (e.g., [2, 34]) we do not impose reciprocal terms in the control input that grow unbounded in order to guarantee closed-loop stability. The resulting controller is essentially a simple linear feedback on e_1, e_2 with time-varying adaptive control gains, accompanied by the neural network output that ensures the growth and boundedness condition (8). Moreover, note that the convergence result of Theorem 1 is independent from the selection of the control gain constants $k_{i,2}, \mu_{i,1}, \mu_{i,2}, i \in \mathcal{N}$, which are only required to be positive. Their selection does affect, however, the performance characteristics of the errors $e_{i,1}, e_{i,2}$ such as overshoot and rate of convergence.

4 NUMERICAL EXPERIMENTS

We consider $N = 5$ follower aerial vehicles in \mathbb{R}^3 with dynamics of the form (1). Details regarding the terms $f_i()$ and $g_i()$ are given in Appendix B. We evaluate the proposed algorithm in three test cases.

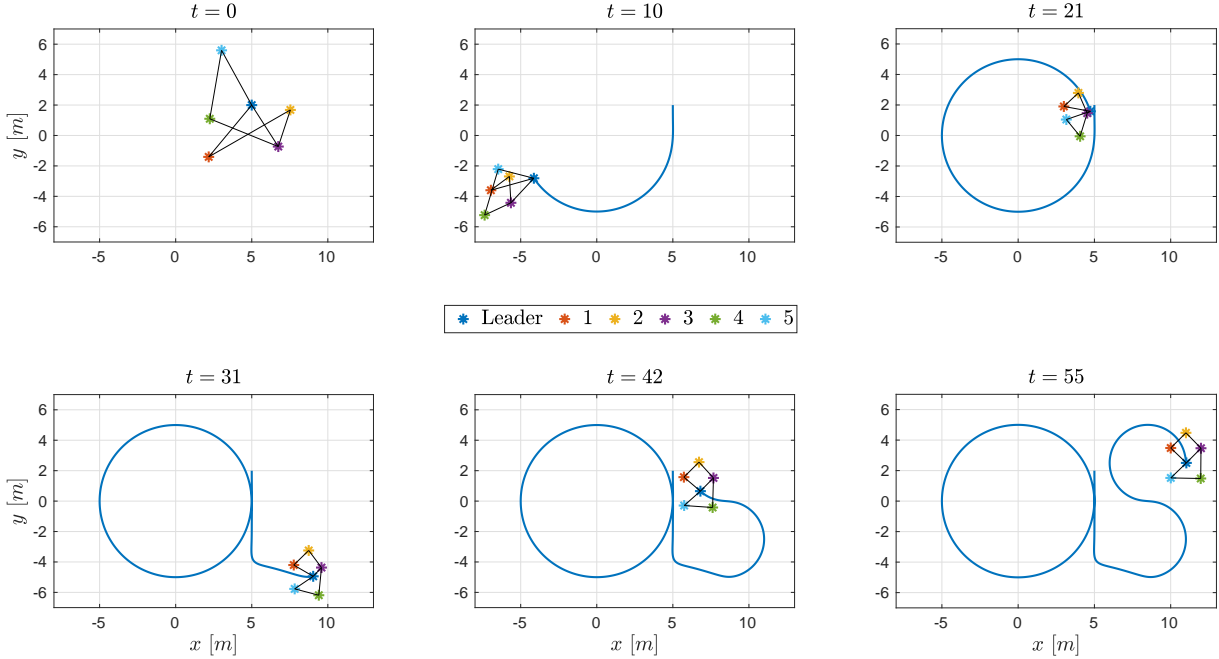


Figure 1: Snapshots of the first experiment in the x - y plane. The agents converge to the desired formation (see bottom-middle and bottom-right plots) around the leader, which follows a pre-specified trajectory (continuous blue line). The black lines represent the communication edge set $\tilde{\mathcal{E}}$ of the agents.

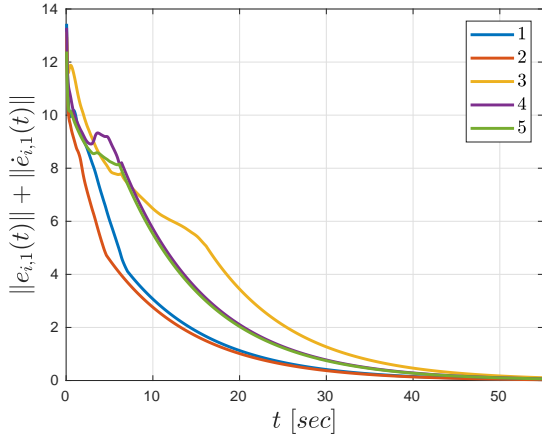


Figure 2: Evolution of the error signals $\|e_{i,1}(t)\| + \|\dot{e}_{i,1}(t)\|$ for $i \in \{1, \dots, 5\}$, and $t \in [0, 55]$, for the first experiment.

The first case consists of the stabilization of the followers around the leader, which is assigned with the tracking of a reference time-varying trajectory profile $x_0(t)$. We consider a communication graph modeled by the edge set $\tilde{\mathcal{E}} = \{(1, 2), (2, 3), (3, 4), (4, 5), (1, 0), (3, 0), (5, 0)\}$, i.e., agents 1, 3, and 5 have access to the information of the leader. The stabilization is dictated by the formation constants c_{ij} , $(i, j) \in \tilde{\mathcal{E}}$, which can be found in Appendix B. The aforementioned parameters, along with the agents' initial conditions, specify the

first task's formation instance $\mathcal{F} := (x_0, \bar{f}, \bar{g}, \bar{c}, \bar{\mathcal{G}}, \bar{x}(0))$. We generate data from 100 trajectories that correspond to different \bar{f} , \bar{g} , $\bar{x}(0)$ than in \mathcal{F} , but with the same leader profile x_0 and inter-agent formation offsets \bar{c} and communication graph $\bar{\mathcal{G}}$, and we train 5 neural networks, one for each agent. We test the control policy (10) using the task's formation instance \mathcal{F} . The results are depicted in Figs. 1-2; Fig. 1 depicts snapshots of the multi-agent formation in the x - y plane and Fig. 2 shows the evolution of the error signals $\|e_{i,1}(t)\| + \|\dot{e}_{i,1}(t)\|$ for $i \in \{1, \dots, 5\}$. One concludes that the multi-agent system converges successfully to the pre-specified formation, which is depicted in the bottom-right plot of Fig. 1¹. More details regarding the experiment can be found in Appendix B.

The second case comprises a surveillance task, where the agents need to periodically surveil three areas in the environment. We choose the same communication graph as in the first case. Each area consists of 6 regions of interest; the leader navigates sequentially to one of the regions in the areas, and by appropriately setting the constants c_{ij} , $(i, j) \in \tilde{\mathcal{E}}$, according to the geometry of the regions, the followers aim to visit the remaining five regions in each area. Similarly to the first case, we generate data from 100 trajectories that correspond to different \bar{f} , \bar{g} , $\bar{x}(0)$ than in the task's formation instance \mathcal{F} , and we train 5 neural networks, one for each agent. We test the control policy (10) on \mathcal{F} , giving the results depicted in Figs. 3-4; Fig. 3 depicts snapshots of the agents' visit to the three areas (at $t = 50$, $t = 150$, and $t = 225$ seconds, respectively), and Fig. 4 depicts the evolution of the signals $\|e_{i,1}(t)\| + \|\dot{e}_{i,1}(t)\|$ for all agents $i \in \{1, \dots, 5\}$. As illustrated in the figures, the agents

¹The agents converge to the same value in the z -coordinate.

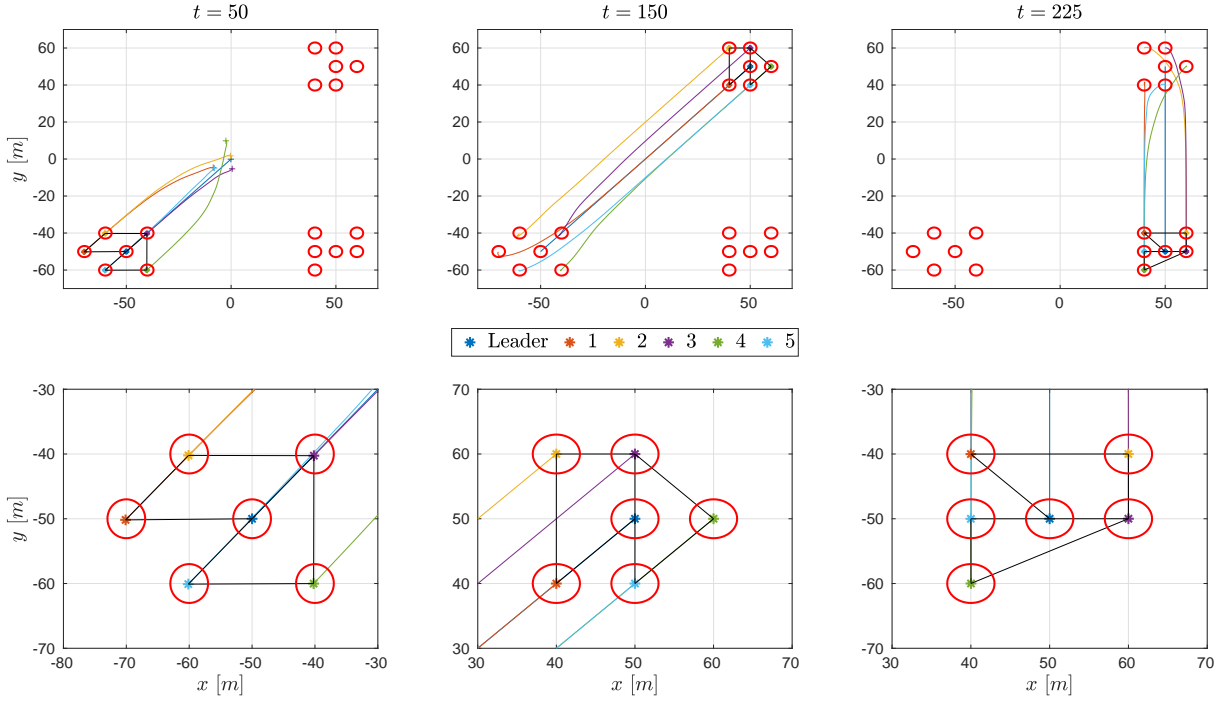


Figure 3: Snapshots of the second experiment (top) and their zoomed-in versions (bottom) in the x - y plane. The agents converge to the desired formation around the leader at $t = 50$, $t = 150$, and $t = 225$, which implies the visit of the regions of interest in the three areas. The black lines represent the communication edge set $\bar{\mathcal{E}}$ of the agents. The initial positions of the agents are depicted with “+” in the top-left plot.

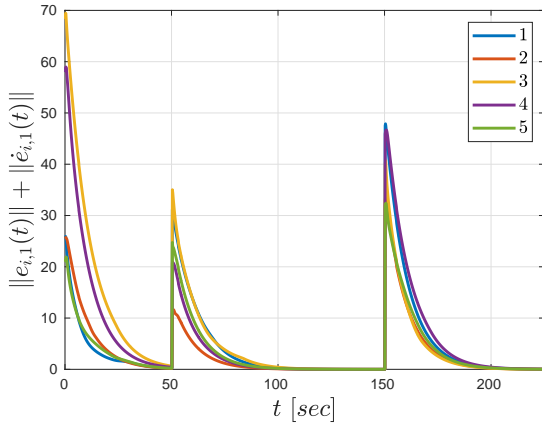


Figure 4: Evolution of the error signals $\|e_{i,1}(t)\| + \|\dot{e}_{i,1}(t)\|$ for $i \in \{1, \dots, 5\}$, and $t \in [0, 225]$, for the second experiment.

converge successfully to the three pre-specified formations, visiting the regions of interest in the three areas. More details regarding the experiment can be found in Appendix B.

The first two cases considered training data that correspond to the exact formation task, defined by the leader profile x_0 and the constants c_{ij} , and communication graph $\bar{\mathcal{G}}$. In the third case, we generate 120 different formation instances $\mathcal{F}^k := (x_0^k, \bar{f}^k, \bar{g}^k, \bar{c}^k, \bar{\mathcal{G}}^k, \bar{x}^k(0))$

$k \in \{1, \dots, 120\}$, i.e., different trajectory profiles for the leader, different terms $f_i()$ and $g_i()$ for the agents, different communication graphs $\bar{\mathcal{G}}$ satisfying Assumption 2, different formation constants c_{ij} , for $(i, j) \in \bar{\mathcal{E}}$, and different initial conditions for the agents. We separate the 120 instances into 100 training and 20 test instances. We train next 5 neural networks, one for each agent, using data from system runs that correspond to the 100 first training instances $\mathcal{F}^k, k \in \{1, \dots, 100\}$. We test the control policy on the 20 first training instances $\mathcal{F}^k, k \in \{1, \dots, 20\}$, as well as on the 20 test instances that were not used in the training, i.e., $\mathcal{F}^k, k \in \{101, \dots, 120\}$. In addition, we compare the performance of the proposed control algorithm with a *no-neural-network* (no-NN) control policy, i.e. a policy that does not employ the neural network, (term $u_{i,nn}$ in (10a)) and with a non-adaptive control policy $u_i = u_{i,nn} - k_{i,2}e_{i,2}$, i.e., without the adaptation terms $\hat{d}_{i,1}, \hat{d}_{i,2}$. The comparison results are given in Fig. 5, which depicts the mean and standard deviation of the signal $\|\dot{e}_1(t)\| + \|\dot{e}_1(t)\|$ for the 20 of the training instances (top), and for the 20 test instances (bottom). In both cases, the proposed control algorithm outperforms the other two policies, which, in many of the instances, resulted in unstable closed-loop systems. More details regarding the experiment can be found in Appendix B.

5 DISCUSSION AND LIMITATIONS

As shown in the experimental results, the distributed control algorithm is able to accomplish formation tasks, even when these

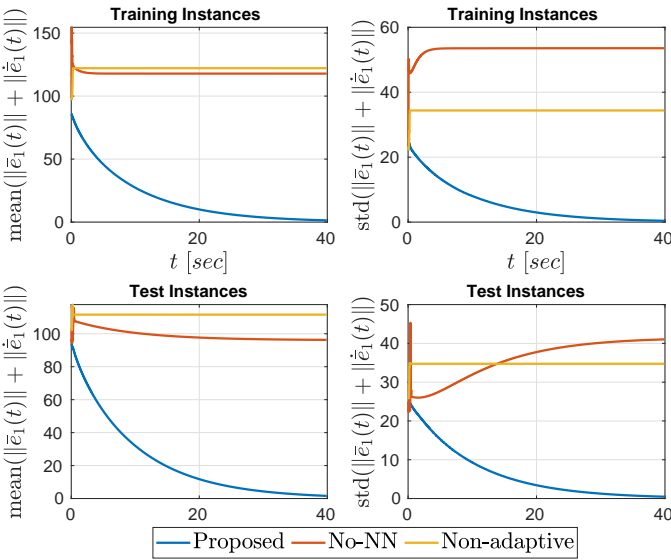


Figure 5: Evolution of the mean (left) and standard deviation (right) of the signals $\|\bar{e}_1(t)\| + \|\dot{\bar{e}}_1(t)\|$ for the 20 training instances (top) and the 20 test instances (bottom).

are not considered when generating the training data. Similarly, the trajectories used in the training data were generated using systems with different agent dynamics and communication graphs, and not specifically the ones used in the tests. The aforementioned attributes signify the ability of the proposed algorithm to generalize to different tasks and systems with different dynamic models and communication topologies. Nevertheless, the proposed control policy is currently restricted to systems of the form (1) satisfying Assumption 1 and is not able to take into account under-actuated systems (e.g., the acrobot or cart-pole system) or systems with non-holonomic constraints; the analysis of such systems consists part of our future work. Finally, the discontinuities of (10a) might be problematic and create chattering when implemented in real actuators. A continuous approximation that has shown to yield satisfying performance is the boundary-layer technique ([29]).

6 CONCLUSION AND FUTURE WORK

We develop a learning-based control algorithm for the formation control of networked multi-agent systems with unknown nonlinear dynamics. The algorithm integrates distributed neural-network-based learning and adaptive control. We provide formal guarantees and perform extensive numerical experiments. Future efforts will focus on relaxing the considered assumptions and extending the proposed methodology to account for directed and time-varying communication graphs as well as underactuated systems.

REFERENCES

- [1] Charalampos P Bechlioulis and Kostas J Kyriakopoulos. 2015. Robust model-free formation control with prescribed performance for nonlinear multi-agent systems. *IEEE International Conference on Robotics and Automation (ICRA)* (2015), 1268–1273.
- [2] Charalampos P Bechlioulis and George A Rovithakis. 2016. Decentralized robust synchronization of unknown high order nonlinear multi-agent systems with prescribed transient and steady state performance. *IEEE Trans. Automat. Control* 62, 1 (2016), 123–134.
- [3] Dimitri Bertsekas. 2021. Lessons from AlphaZero for Optimal, Model Predictive, and Adaptive Control. *arXiv preprint arXiv:2108.10315* (2021).
- [4] Ci Chen, Changyun Wen, Zhi Liu, Kan Xie, Yun Zhang, and CL Philip Chen. 2016. Adaptive consensus of nonlinear multi-agent systems with non-identical partially unknown control directions and bounded modelling errors. *IEEE Trans. Automat. Control* 62, 9 (2016), 4654–4659.
- [5] Iain D Couzin, Jens Krause, Nigel R Franks, and Simon A Levin. 2005. Effective leadership and decision-making in animal groups on the move. *Nature* 433, 7025 (2005), 513–516.
- [6] George Cybenko. 1989. Approximation by superpositions of a sigmoidal function. *Mathematics of control, signals and systems* 2, 4 (1989), 303–314.
- [7] Emiliano Dall’Anese, Hao Zhu, and Georgios B Giannakis. 2013. Distributed optimal power flow for smart microgrids. *IEEE Transactions on Smart Grid* 4, 3 (2013), 1464–1475.
- [8] Thinh Doan, Siva Maguluri, and Justin Romberg. 2019. Finite-time analysis of distributed TD (0) with linear function approximation on multi-agent reinforcement learning. *International Conference on Machine Learning* (2019), 1626–1635.
- [9] Yang Fei, Peng Shi, and Cheng-Chew Lim. 2020. Neural network adaptive dynamic sliding mode formation control of multi-agent systems. *International Journal of Systems Science* 51, 11 (2020), 2025–2040.
- [10] Nicholas Fischer, Rushikesh Kamalapurkar, and Warren E Dixon. 2013. LaSalle-Yoshizawa corollaries for nonsmooth systems. *IEEE Trans. Automat. Control* 58, 9 (2013), 2333–2338.
- [11] Jakob Foerster, Nantas Nardelli, Gregory Farquhar, Triantafyllos Afouras, Philip HS Torr, Pushmeet Kohli, and Shimon Whiteson. 2017. Stabilising experience replay for deep multi-agent reinforcement learning. *International conference on machine learning* (2017), 1146–1155.
- [12] Jakob N Foerster, Yannis M Assael, Nando De Freitas, and Shimon Whiteson. 2016. Learning to communicate with deep multi-agent reinforcement learning. *arXiv preprint arXiv:1605.06676* (2016).
- [13] Jayesh K Gupta, Maxim Egorov, and Mykel Kochenderfer. 2017. Cooperative multi-agent control using deep reinforcement learning. *International Conference on Autonomous Agents and Multiagent Systems* (2017), 66–83.
- [14] Eric A Hansen, Daniel S Bernstein, and Shlomo Zilberman. 2004. Dynamic programming for partially observable stochastic games. *AAAI* 4 (2004), 709–715.
- [15] Pablo Hernandez-Leal, Bilal Kartal, and Matthew E Taylor. 2019. A survey and critique of multiagent deep reinforcement learning. *Autonomous Agents and Multi-Agent Systems* 33, 6 (2019), 750–797.
- [16] Jiangping Hu and Wei Xing Zheng. 2014. Adaptive tracking control of leader-follower systems with unknown dynamics and partial measurements. *Automatica* 50, 5 (2014), 1416–1423.
- [17] SN Huang, Kok Kiong Tan, and Tong Heng Lee. 2006. Nonlinear adaptive control of interconnected systems using neural networks. *IEEE Transactions on Neural Networks* 17, 1 (2006), 243–246.
- [18] Ali Jadbabaie, Jie Lin, and A Stephen Morse. 2003. Coordination of groups of mobile autonomous agents using nearest neighbor rules. *IEEE Transactions on automatic control* 48, 6 (2003), 988–1001.
- [19] Soumyya Kar, José MF Moura, and H Vincent Poor. 2013. QD-Learning: A Collaborative Distributed Strategy for Multi-Agent Reinforcement Learning Through Consensus and Innovations. *IEEE Transactions on Signal Processing* 61 (2013), 1848–1862.
- [20] M. Krstic, I. Kanellakopoulos, and P. Kokotovic. 1995. Nonlinear and Adaptive Control Design. *Publisher Wiley New York* (1995).
- [21] Frank L Lewis, Hongwei Zhang, Kristian Hengster-Movric, and Abhijit Das. 2013. *Cooperative control of multi-agent systems: optimal and adaptive design approaches*. Springer Science & Business Media.
- [22] Derong Liu, Chao Li, Hongliang Li, Ding Wang, and Hongwen Ma. 2015. Neural-network-based decentralized control of continuous-time nonlinear interconnected systems with unknown dynamics. *Neurocomputing* 165 (2015), 90–98.
- [23] Xi Ma, Fuchun Sun, Hongbo Li, and Bing He. 2017. Neural-network-based integral sliding-mode tracking control of second-order multi-agent systems with unmatched disturbances and completely unknown dynamics. *International Journal of Control, Automation and Systems* 15, 4 (2017), 1925–1935.
- [24] Hamidreza Modares, Frank L Lewis, Wei Kang, and Ali Davoudi. 2017. Optimal synchronization of heterogeneous nonlinear systems with unknown dynamics. *IEEE Trans. Automat. Control* 63, 1 (2017), 117–131.
- [25] Junkang Ni and Peng Shi. 2020. Adaptive neural network fixed-time leader-follower consensus for multiagent systems with constraints and disturbances. *IEEE transactions on cybernetics* 51, 4 (2020), 1835–1848.
- [26] Reza Olfati-Saber, J Alex Fax, and Richard M Murray. 2007. Consensus and cooperation in networked multi-agent systems. *Proc. IEEE* 95, 1 (2007), 215–233.
- [27] Shayegan Omidshafiei, Jason Pazis, Christopher Amato, Jonathan P How, and John Vian. 2017. Deep decentralized multi-task multi-agent reinforcement learning under partial observability. (2017), 2681–2690.
- [28] Brad Paden and Shankar Sastry. 1987. A calculus for computing Filippov’s differential inclusion with application to the variable structure control of robot manipulators. *IEEE transactions on circuits and systems* 34, 1 (1987), 73–82.

[29] Jean-Jacques E Slotine, Weiping Li, et al. 1991. *Applied nonlinear control*. Vol. 199. Prentice hall Englewood Cliffs, NJ.

[30] Kyriakos G Vamvoudakis and Frank L Lewis. 2011. Multi-player non-zero-sum games: Online adaptive learning solution of coupled Hamilton–Jacobi equations. *Automatica* 47, 8 (2011), 1556–1569.

[31] Kyriakos G Vamvoudakis, Hamidreza Modares, Bahare Kiumarsi, and Frank L Lewis. 2017. Game theory-based control system algorithms with real-time reinforcement learning: How to solve multiplayer games online. *IEEE Control Systems Magazine* 37, 1 (2017), 33–52.

[32] Christos K Verginis, Charalampos P Bechlioulis, Dimos V Dimarogonas, and Kostas J Kyriakopoulos. 2017. Robust distributed control protocols for large vehicular platoons with prescribed transient and steady-state performance. *IEEE Transactions on Control Systems Technology* 26, 1 (2017), 299–304.

[33] Christos K Verginis and Dimos V Dimarogonas. 2019. Adaptive leader-follower coordination of lagrangian multi-agent systems under transient constraints. *IEEE 58th Conference on Decision and Control (CDC)* (2019), 3833–3838.

[34] Christos K Verginis, Alexandros Nikou, and Dimos V Dimarogonas. 2019. Robust formation control in SE (3) for tree-graph structures with prescribed transient and steady state performance. *Automatica* 103 (2019), 538–548.

[35] Hoi-To Wai, Zhuoran Yang, Zhaoran Wang, and Mingyi Hong. 2018. Multi-agent reinforcement learning via double averaging primal-dual optimization. *arXiv preprint arXiv:1806.00877* (2018).

[36] Xiaofeng Wang and Tuomas Sandholm. 2002. Reinforcement learning to play an optimal Nash equilibrium in team Markov games. *Advances in neural information processing systems* 15 (2002), 1603–1610.

[37] Yujuan Wang, Yongduan Song, and Wei Ren. 2017. Distributed adaptive finite-time approach for formation-containment control of networked nonlinear systems under directed topology. *IEEE transactions on neural networks and learning systems* 29, 7 (2017), 3164–3175.

[38] Guoxing Wen, CL Philip Chen, Yan-Jun Liu, and Zhi Liu. 2016. Neural network-based adaptive leader-following consensus control for a class of nonlinear multiagent state-delay systems. *IEEE transactions on cybernetics* 47, 8 (2016), 2151–2160.

[39] Hongwei Zhang and Frank L Lewis. 2012. Adaptive cooperative tracking control of higher-order nonlinear systems with unknown dynamics. *Automatica* 48, 7 (2012), 1432–1439.

[40] Kaiqing Zhang, Yang Liu, Ji Liu, Mingyan Liu, and Tamer Başar. 2020. Distributed learning of average belief over networks using sequential observations. *Automatica* 115 (2020), 108857.

[41] Kaiqing Zhang, Liquan Lu, Chao Lei, Hao Zhu, and Yanfeng Ouyang. 2018. Dynamic operations and pricing of electric unmanned aerial vehicle systems and power networks. *Transportation Research Part C: Emerging Technologies* 92 (2018), 472–485.

[42] Kaiqing Zhang, Zhuoran Yang, and Tamer Başar. 2021. Multi-agent reinforcement learning: A selective overview of theories and algorithms. *Handbook of Reinforcement Learning and Control* (2021), 321–384.

A APPENDIX

We provide here the proof of Theorem 1. We first give some preliminary notation and background on non-smooth systems.

Notation

Given a function $f : \mathbb{R}^n \rightarrow \mathbb{R}^k$, its Filippov regularization is defined as [28]

$$K[f](x) := \bigcap_{\delta > 0} \bigcap_{\mu(\bar{N})=0} \overline{\text{co}}(f(O(x, \delta) \setminus \bar{N}), t), \quad (11)$$

where $\bigcap_{\mu(\bar{N})=0}$ is the intersection over all sets \bar{N} of Lebesgue measure zero, $\overline{\text{co}}(E)$ is the closure of the convex hull $\text{co}(E)$ of the set E , and $O(x, \delta)$ denotes the ball of radius δ centered at x .

Nonsmooth Analysis

Let the differential equation with a discontinuous right-hand side:

$$\dot{x} = f(x, t), \quad (12)$$

where $f : \mathcal{D} \times [t_0, \infty) \rightarrow \mathbb{R}^n$, $\mathcal{D} \subset \mathbb{R}^n$, is Lebesgue measurable and locally essentially bounded.

DEFINITION 1 (DEF. 1 OF [10]). A function $x : [t_0, t_1] \rightarrow \mathbb{R}^n$, with $t_1 > t_0$, is called a Filippov solution of (12) on $[t_0, t_1]$ if $x(t)$ is absolutely continuous and if, for almost all $t \in [t_0, t_1]$, it satisfies $\dot{x} \in K[f](x, t)$, where $K[f](x, t)$ is the Filippov regularization of $f(x, t)$.

LEMMA 1 (LEMMA 1 OF [10]). Let $x(t)$ be a Filippov solution of (12) and $V : \mathcal{D} \times [t_0, t_1] \rightarrow \mathbb{R}$ be a locally Lipschitz, regular function². Then $V(x(t), t)$ is absolutely continuous, $\dot{V}(x(t), t) = \frac{\partial}{\partial t} V(x(t), t)$ exists almost everywhere (a.e.), i.e., for almost all $t \in [t_0, t_1]$, and $\dot{V}(x(t), t) \stackrel{a.e.}{\in} \dot{V}(x(t), t)$, where

$$\dot{V} := \bigcap_{\xi \in \partial V(x, t)} \xi^\top \begin{bmatrix} K[f](x, t) \\ 1 \end{bmatrix},$$

and $\partial V(x, t)$ is Clarke's generalized gradient at (x, t) [10].

COROLLARY 1 (COROLLARY 2 OF [10]). For the system given in (12), let $\mathcal{D} \subset \mathbb{R}^n$ be an open and connected set containing $x = 0$ and suppose that f is Lebesgue measurable and $x \mapsto f(x, t)$ is essentially locally bounded, uniformly in t . Let $V : \mathcal{D} \times [t_0, t_1] \rightarrow \mathbb{R}$ be locally Lipschitz and regular such that $W_1(x) \leq V(x, t) \leq W_2(x)$, $\forall t \in [t_0, t_1], x \in \mathcal{D}$, and

$$z \leq -W(x(t)), \quad \forall z \in \dot{V}(x(t), t), \quad t \in [t_0, t_1], \quad x \in \mathcal{D},$$

where W_1 and W_2 are continuous positive definite functions and W is a continuous positive semi-definite on \mathcal{D} . Choose $r > 0$ and $c > 0$ such that $\bar{\mathcal{B}}(0, r) \subset \mathcal{D}$ and $c < \min_{\|x\|=r} W_1(x)$. Then for all Filippov solutions $x : [t_0, t_1] \rightarrow \mathbb{R}^n$ of (12), with $x(t_0) \in \mathcal{D} := \{x \in \bar{\mathcal{B}}(0, r) : W_2(x) \leq c\}$, it holds that $t_1 = \infty$, $x(t) \in \mathcal{D}$, $\forall t \in [t_0, \infty)$, and $\lim_{t \rightarrow \infty} W(x(t)) = 0$.

PROOF OF THEOREM 1. Since the control algorithm is discontinuous, we use the notion of Filippov solutions. The Filippov regularization of u_i is $K[u_i] = u_{i,nn}(\bar{x}) - (k_{i,1} + \hat{d}_{i,1})e_{i,2} - k_{i,1}\hat{d}_{i,2}\hat{E}_{i,2}$, where $\hat{E}_{i,2} := \frac{e_{i,2}}{\|e_{i,2}\|}$ if $e_{i,2} \neq 0$ and $\hat{E}_{i,2} \in (-1, 1)^n$ otherwise. Note that, in any case, it holds that $e_{i,2}^\top \hat{E}_{i,2} = \|e_{i,2}\|$, for all $i \in \mathcal{N}$.

Let now the continuously differentiable function

$$V_1(\bar{e}) := \frac{1}{2} \|\bar{e}_1\|^2 + \frac{1}{2g} \bar{e}_2^\top H^{-1} \bar{e}_2$$

where $\bar{e} := [\bar{e}_1^\top, \bar{e}_2^\top]^\top$, $\underline{g} := \min_{i \in \mathcal{N}} \{\lambda_{\min}(g_i)\}$, and λ_{\min} is the minimum-eigenvalue operator. Note that \underline{g} is positive due to Assumption 1. According to Lemma 1, $\dot{V}_1 \stackrel{a.e.}{\in} \dot{V}_1$, with $\dot{V}_1 := \bigcap_{\xi \in \partial V_1} K[\dot{\bar{e}}]$. Since $V_1(\bar{e})$ is continuously differentiable, its generalized gradient reduces to the standard gradient and thus it holds that $\dot{V}_1(\bar{e}) = \nabla V_1^\top K[\dot{\bar{e}}]$, where $\nabla V_1 = [\bar{e}_1^\top, \frac{1}{g} \bar{e}_2^\top H^{-1}]^\top$. By differentiating V_1 and using (9), one obtains

$$\dot{V}_1 \subset \widetilde{W}_1 := \bar{e}_1^\top \dot{\bar{e}}_1 + \frac{1}{g} \bar{e}_2^\top H^{-1} (\bar{K}_1 \dot{\bar{e}}_1 + \ddot{\bar{e}}_1)$$

²See [10] for a definition of regular functions.

where $\bar{K}_1 := \text{diag}\{k_{1,1}, \dots, k_{N,1}\}$, and by further using (2),

$$\begin{aligned}\tilde{W}_1 &= -\bar{e}_1^\top \bar{K}_1 \bar{e}_1 + \bar{e}_1^\top \bar{e}_2 + \frac{1}{\underline{g}} \bar{e}_2^\top H^{-1} \left(\bar{K}_1 \bar{e}_2 - \bar{K}_1^2 \bar{e}_1 \right. \\ &\quad \left. + H(\bar{f} + \bar{g}\bar{u} - \dot{\bar{x}}_{0,2}) \right) \\ &= -\bar{e}_1^\top \bar{K}_1 \bar{e}_1 + \bar{e}_1^\top B \bar{e}_2 + \frac{1}{\underline{g}} \bar{e}_2^\top H^{-1} \bar{K}_1 \bar{e}_2 + \frac{1}{\underline{g}} \bar{e}_2^\top (\bar{f} + \bar{g}\bar{u} - \dot{\bar{x}}_{0,2})\end{aligned}$$

where we have defined $B := I_{Nn} - \frac{1}{\underline{g}} \bar{K}_1^2 H^{-1}$. In view of (10a), the term $\frac{1}{\underline{g}} \bar{e}_2^\top (\bar{f} + \bar{g}\bar{u})$ expands to

$$\begin{aligned}\frac{1}{\underline{g}} \bar{e}_2^\top (\bar{f} + \bar{g}\bar{u}) &= \frac{1}{\underline{g}} \sum_{i \in \mathcal{N}} e_{i,2}^\top (f_i + g_i u_i) \\ &= -\frac{1}{\underline{g}} \sum_{i \in \mathcal{N}} e_{i,2}^\top g_i \left((k_{i,2} + \hat{d}_{i,1}) e_{i,2} + \hat{d}_{i,2} \hat{e}_{i,2} \right) + \frac{1}{\underline{g}} \bar{e}_2^\top (\bar{f} + \bar{g}\bar{u}_{nn}) \\ &\leq -\sum_{i \in \mathcal{N}} \left((k_{i,2} + \hat{d}_{i,1}) \|e_{i,2}\|^2 + \hat{d}_{i,2} \|e_{i,2}\| \right) + \frac{1}{\underline{g}} \bar{e}_2^\top (\bar{f} + \bar{g}\bar{u}_{nn})\end{aligned}$$

where we have used the positive definiteness of g_i , $i \in \mathcal{N}$, and the fact that $\underline{g} = \min_{i \in \mathcal{N}} \{\lambda_{\min}(g_i)\}$. We now re-write inequality (8) of Assumption 3. According to (3) and (9), as well as the positive definiteness of $H = (\mathcal{L} + \mathcal{B}) \otimes I_n$, one obtains

$$\begin{aligned}\|\bar{x}_1\| &\leq \|\bar{x}_1 - \bar{x}_{0,1}(t) + \bar{c}\| + \|\bar{x}_{0,1}(t)\| + \|\bar{c}\| \\ &\leq \|H^{-1}\| \|e_1\| + \|\bar{x}_{0,1}(t)\| + \|\bar{c}\| \\ \|\bar{x}_2\| &\leq \|H^{-1}\| \|\dot{e}_1\| + \|\bar{x}_{0,2}(t)\| \\ &\leq k_1 \|H^{-1}\| \|e_2\| + k_1 \|H^{-1}\| \|e_1\| + \|\bar{x}_{0,2}(t)\|\end{aligned}$$

Hence, since $\bar{x}_{0,1}$, $\bar{x}_{0,2}$, and $\dot{\bar{x}}_{0,2}$ are bounded functions of time, (8) implies that there exist positive constants ζ_1, ζ_2, Z such that

$$\frac{1}{\underline{g}} \|\bar{f}(\bar{x}, t) + \bar{g}(\bar{x}, t) \bar{u}_{nn}(\bar{x}) - \dot{\bar{x}}_{0,2}(t)\| \leq \zeta_1 \|e_1\| + \zeta_2 \|e_2\| + Z \quad (13)$$

Therefore, \tilde{W}_1 becomes

$$\begin{aligned}\tilde{W}_1 &\leq -\bar{e}_1^\top \bar{K}_1 \bar{e}_1 + \bar{b} \|\bar{e}_1\| \|\bar{e}_2\| + \bar{h} \|\bar{e}_2\|^2 - \sum_{i \in \mathcal{N}} \left((k_{i,2} + \hat{d}_{i,1}) \|e_{i,2}\|^2 \right. \\ &\quad \left. + \hat{d}_{i,2} \|e_{i,2}\| \right) + \zeta_1 \|\bar{e}_1\| \|\bar{e}_2\| + \zeta_2 \|\bar{e}_2\|^2 + Z \|\bar{e}_2\|,\end{aligned}$$

where we further define $\bar{b} := \|B\|$, and $\bar{h} := \frac{1}{\underline{g}} \|H^{-1} \bar{K}_1\|$. Let now a positive constant γ such that the matrix $\bar{A} := \bar{K}_1 - \gamma \frac{\bar{b} + \zeta_1}{2} I_{Nn}$ is positive definite. By using the property $\alpha\beta \leq \frac{\alpha^2}{2} + \frac{\beta^2}{2}$ for any constants α, β , we re-write the term $\bar{b} \|\bar{e}_1\| \|\bar{e}_2\|$ as $\gamma \bar{b} \|\bar{e}_1\| \frac{\|\bar{e}_2\|}{\gamma} \leq \frac{\gamma \bar{b}}{2} \|\bar{e}_1\|^2 + \frac{\bar{b}}{2\gamma} \|\bar{e}_2\|^2$. Similarly, by writing $\zeta_1 \|\bar{e}_1\| \|\bar{e}_2\| \leq \frac{\zeta_1}{2} \|\bar{e}_1\|^2 + \frac{\zeta_1}{2} \|\bar{e}_2\|^2$ and defining $d_1 := \frac{\bar{b}}{2\gamma} + \frac{\zeta_1}{2} + \bar{h} + \zeta_2$, $d_2 := Z$, \tilde{W}_1 becomes

$$\begin{aligned}\tilde{W}_1 &\leq -\bar{e}_1^\top \bar{A} \bar{e}_1 + d_1 \|e_2\|^2 + d_2 \|e_2\| - \sum_{i \in \mathcal{N}} \left((k_{i,2} + \hat{d}_{i,1}) \|e_{i,2}\|^2 \right. \\ &\quad \left. + \hat{d}_{i,2} \|e_{i,2}\| \right)\end{aligned}$$

and by using $\|\bar{e}_2\|^2 = \sum_{i \in \mathcal{N}} \|e_{i,2}\|^2$, $\|\bar{e}_2\| \leq \sum_{i \in \mathcal{N}} \|e_{i,2}\|$,

$$\begin{aligned}\tilde{W}_1 &\leq -\bar{e}_1^\top \bar{A} \bar{e}_1 + d_1 \sum_{i \in \mathcal{N}} \|e_{i,2}\|^2 + d_2 \sum_{i \in \mathcal{N}} \|e_{i,2}\| \\ &\quad - \sum_{i \in \mathcal{N}} \left((k_{i,2} + \hat{d}_{i,1}) \|e_{i,2}\|^2 + \hat{d}_{i,2} \|e_{i,2}\| \right) \quad (14)\end{aligned}$$

In view of the aforementioned expression, the individual adaptation variables $\hat{d}_{i,1}$ and $\hat{d}_{i,2}$, for all $i \in \mathcal{N}$, aim to approximate d_1 and d_2 , respectively. Therefore, define the adaptation errors $\tilde{d}_1 := [\tilde{d}_{1,1}, \dots, \tilde{d}_{N,1}]^\top := [\hat{d}_{1,1} - d_1, \dots, \hat{d}_{N,1} - d_1]^\top$, $\tilde{d}_2 := [\tilde{d}_{1,2}, \dots, \tilde{d}_{N,2}]^\top := [\hat{d}_{1,2} - d_2, \dots, \hat{d}_{N,2} - d_2]^\top$ and the overall state $\tilde{x} := [\bar{e}_1^\top, \bar{e}_2^\top, \tilde{d}_1^\top, \tilde{d}_2^\top]^\top \in \mathbb{R}^{2N(n+1)}$. Let the continuously differentiable function

$$V_2(\tilde{x}) := V_1(\tilde{x}) + \frac{1}{2} \tilde{d}_1^\top \tilde{M}_1^{-1} \tilde{d}_1 + \frac{1}{2} \tilde{d}_2^\top \tilde{M}_2^{-1} \tilde{d}_2$$

where $\tilde{M}_1 := \text{diag}\{\mu_{1,1}, \dots, \mu_{N,1}\}$, $\tilde{M}_2 := \text{diag}\{\mu_{1,2}, \dots, \mu_{N,2}\}$; note that $V_2(\tilde{x})$ satisfies $W_{\underline{m}}(\tilde{x}) \leq V_2(\tilde{x}) \leq W_{\bar{m}}(\tilde{x})$, where $W_{\underline{m}}(\tilde{x}) := \underline{m} \|\tilde{x}\|^2$, $W_{\bar{m}}(\tilde{x}) := \bar{m} \|\tilde{x}\|^2$ for some positive constants \underline{m}, \bar{m} . By differentiating V_2 and following similar steps with V_1 and using (14), we obtain

$$\begin{aligned}\dot{\tilde{V}}_2 \subset \tilde{W}_2 &\leq -\bar{e}_1^\top \bar{A} \bar{e}_1 + d_1 \sum_{i \in \mathcal{N}} \|e_{i,2}\|^2 + d_2 \sum_{i \in \mathcal{N}} \|e_{i,2}\| \\ &\quad - \sum_{i \in \mathcal{N}} \left((k_{i,2} + \hat{d}_{i,1}) \|e_{i,2}\|^2 + \hat{d}_{i,2} \|e_{i,2}\| \right) \\ &\quad + \sum_{i \in \mathcal{N}} \left(\frac{1}{\mu_{i,1}} \tilde{d}_{i,1} \dot{\hat{d}}_{i,1} + \frac{1}{\mu_{i,2}} \tilde{d}_{i,2} \dot{\hat{d}}_{i,2} \right)\end{aligned}$$

and by substituting (10b)

$$\dot{\tilde{V}}_2 \subset \tilde{W}_2 \leq -\bar{e}_1^\top \bar{A} \bar{e}_1 - \sum_{i \in \mathcal{N}} k_{i,2} \|e_{i,2}\|^2 =: -W_Q(\tilde{x})$$

Therefore, it holds that $\xi \leq -W_Q(\tilde{x})$, for all $\xi \in \dot{\tilde{V}}_2$, with W_Q being a continuous and positive semi-definite function in $\mathbb{R}^{2N(n+1)}$. Choose now any finite $r > 0$ and let $c < \min_{\|\tilde{x}\|=r} W_{\underline{m}}(\tilde{x})$. All the conditions of Corollary 1 are satisfied and hence, all Filippov solutions starting from $\tilde{x}(0) \in \Omega_f := \{\tilde{x} \in \mathcal{B}(0, r) : \tilde{W}_{\bar{m}}(\tilde{x}) \leq c\}$ are bounded and remain in Ω_f , satisfying $\lim_{t \rightarrow \infty} W_Q(\tilde{x}(t)) = 0$. The boundedness of \tilde{x} implies the boundedness of $\bar{e}_1, \dot{\bar{e}}_2, \tilde{d}_1$, and \tilde{d}_2 , and hence of $\hat{d}_{i,1}(t)$ and $\hat{d}_{i,2}(t)$, for all $t \in \mathbb{R}_{\geq 0}$ and $i \in \mathcal{N}$. In view of (5), we finally conclude the boundedness of $u_i(\cdot)$, $\dot{\hat{d}}_{i,1}$, and $\dot{\hat{d}}_{i,2}$, for all $t \in \mathbb{R}_{\geq 0}$ and $i \in \mathcal{N}$, leading to the conclusion of the proof. \square

B APPENDIX

We provide here more details on the three numerical experiments of Section 4. Regarding the dynamic model (1) of the agents, we set the functions $f_i()$ and $g_i()$ as

$$\begin{aligned}f_i(x_i, t) &= \frac{1}{m_i} (\bar{g}_r + d_{i,1}(t) + d_{i,2}(x_i)) \\ g_i(x_i, t) &= \frac{1}{m_i} I_3\end{aligned}$$

where $\bar{g}_r = [0, 0, 1]^\top$ is the gravity vector, $I_3 \in \mathbb{R}^{3 \times 3}$ is the identity matrix, $m_i \in \mathbb{R}$ is the mass of agent i , and $d_{i,1}(t), d_{i,2}(x_i)$ are chosen

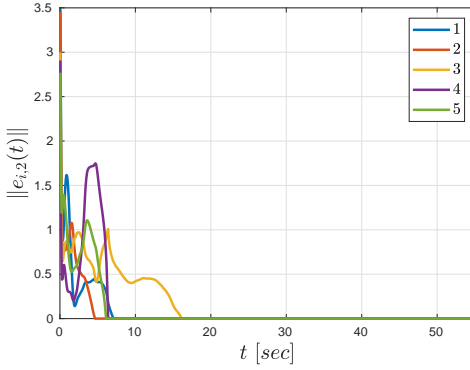


Figure 6: The evolution of the error norms $\|e_{i,2}(t)\|$ for $i \in \{1, \dots, 5\}$, and the first numerical experiment.

as

$$d_{i,1}(t) = \begin{bmatrix} A_{i,1} \sin(\eta_{i,1}t + \phi_{i,1}) \\ A_{i,2} \sin(\eta_{i,2}t + \phi_{i,2}) \\ A_{i,3} \sin(\eta_{i,3}t + \phi_{i,3}) \end{bmatrix}$$

$$d_{i,2}(x_i) = F_i y_i$$

with $y_i = [x_{i,1}^2, x_{i,2}^2, x_{i,3}^2, x_{i,1}x_{i,2}, x_{i,1}x_{i,3}, x_{i,2}x_{i,3}]$, and we further use the notation $x_{i,2} = [x_{i,1}, x_{i,2}, x_{i,3}]^\top$ for all $i \in \mathcal{N}$. The terms $m_i, A_{i,\ell}, \eta_{i,\ell}, \phi_{i,\ell}$ are constants that take values in $(0, 1)$; similarly, $F_i \in \mathbb{R}^{3 \times 6}$ is a constant matrix whose elements take values in $(0, 1)$. For each formation instance that we generate in the numerical experiments, we assign random values to the aforementioned constants. For the execution of the trajectories that are used in the training of the neural networks, we use the control policies

$$u_i(\bar{x}, t) = g_i(x_i, t)^{-1}(u_0(t) - e_{i,2} - f_i(x_i, t))$$

for each agent $i \in \mathcal{N}$. The control gains of the proposed policy (10) are chosen as $k_{i,1} = 0.1, k_{i,2} = \mu_{i,1} = \mu_{i,2} = 0.5$. In all three cases, the data for the training of the neural networks consist of 100 system trajectories, sampled at 500 points, making a total of 50000 points. The neural networks we use in all cases consist of 4 fully connected layers of 512 neurons; each layer is followed by a batch normalization module and a ReLU activation function. For the training we use the adam optimizer, the mean-square-error loss function, and learning rate of 10^{-3} . We further use a batch size of 256, and we train the neural networks until an average (per batch) loss of the order of 10^{-4} is achieved.

Case 1: For the first experiment, we set the desired formation offsets as

$$c_{1,2} = -c_{2,1} = [1, 1, 0]^\top$$

$$c_{2,3} = -c_{3,2} = [1, -1, 0]^\top$$

$$c_{3,4} = -c_{4,3} = [0, -2, 0]^\top$$

$$c_{4,5} = -c_{5,4} = [-2, 0, 0]^\top$$

$$c_{1,0} = [1, -1, 0]^\top$$

$$c_{3,0} = [-1, -1, 0]^\top$$

$$c_{5,0} = [1, 1, 0]^\top$$

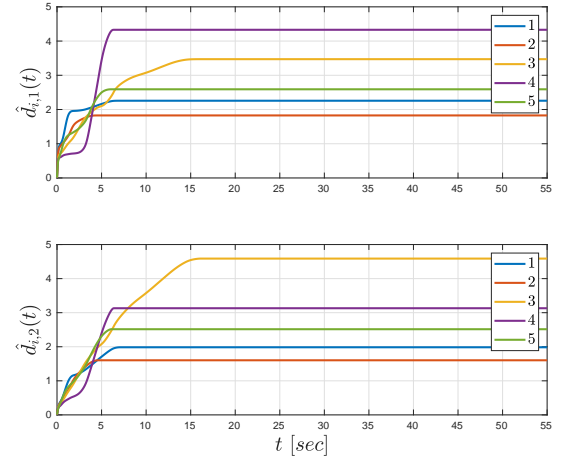


Figure 7: The evolution of the adaptation signals $\hat{d}_{i,1}(t)$ and $\hat{d}_{i,2}(t)$ for $i \in \{1, \dots, 5\}$, and the first numerical experiment.

The task formation instance as well as each formation instance for the generation of the trajectories for the training of the neural networks is created by assigning to the constants $m_i, A_{i,\ell}, \eta_{i,\ell}, \phi_{i,\ell}$ and the elements of F_i a random value in $(0, 1)$, and an initial agent condition for each agent as $x_{i,1}(0) = x_{0,1}(0) + \text{rand}(-4, 4)\bar{1}_3$, $x_{i,2}(0) = \text{rand}(-2, 2)\bar{1}_3$, where $\text{rand}(-a, a)$ denotes the function assigning random values from $-a$ to a and $\bar{1}_3$ denotes the 3-dimensional vector of ones. The formation offsets and communication graph $\bar{\mathcal{G}}$ are the same in all cases (as specified above and in the main manuscript, respectively). The initial condition of the leader is always taken as $x_{0,1}(0) = [5, 2, 10]^\top$, $x_{0,2}(0) = [0.0039, -0.9836, 0]^\top$. The trajectory of the leader in the x - y plane is depicted in Fig. 1 of the main manuscript, whereas it is always equal to 10 meters along the vertical z direction. The total duration of the leader's trajectory is 55 seconds. More results of the first experiment are given in Figs. 6-8. More specifically, Fig. 6 depicts the error norms $\|e_{i,2}(t)\|$, which converge to zero, and Fig. 7 depicts the adaptation signals $\hat{d}_{i,1}(t)$, $\hat{d}_{i,2}(t)$, which converge to a constant value, as soon as $e_{i,2}$ converge to zero, for $i \in \{1, \dots, 5\}$. Finally, Fig. 8 depicts the control inputs u_i of the agents, as well as the respective outputs $u_{i,nn}$ of the neural networks. Note that u_i slowly converge to $u_{i,nn}$ as $e_{i,2}$ converge to zero, as can be also verified by the control policy (10).

Case 2: For the second experiment, we set the regions of interest of the first area at $[-50, -50, -10]^\top, [-70, -50, 10]^\top, [-60, -40, 10]^\top, [-40, -40, 10]^\top, [-40, -60, 10]^\top, [-60, -60, 10]^\top$, and the desired formation offsets as

$$c_{1,2} = -c_{2,1} = [10, 10, 0]^\top$$

$$c_{2,3} = -c_{3,2} = [20, 0, 0]^\top$$

$$c_{3,4} = -c_{4,3} = [0, -20, 0]^\top$$

$$c_{4,5} = -c_{5,4} = [-20, 0, 0]^\top$$

$$c_{1,0} = [20, 0, 0]^\top$$

$$c_{3,0} = [-10, -10, 0]^\top$$

$$c_{5,0} = [10, 10, 0]^\top$$

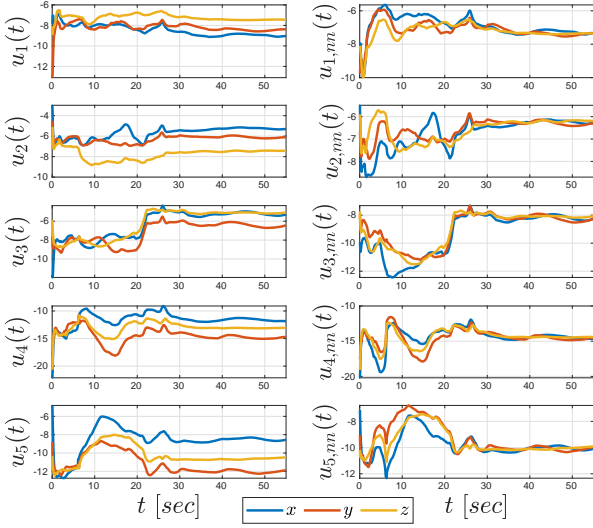


Figure 8: The evolution of the control inputs $u_i(t)$ (left) and the neural-network controllers $u_{i,nn}(t)$ (right), for $i \in \{1, \dots, 5\}$, and the first numerical experiment.

For the second area, we set the regions of interest at $[50, 50, 10]^\top$, $[40, 40, 10]^\top$, $[40, 60, 10]^\top$, $[50, 60, 10]^\top$, $[60, 50, 10]^\top$, $[50, 40, 10]^\top$, and the desired formation offsets as

$$\begin{aligned} c_{1,2} &= -c_{2,1} = [0, 20, 0]^\top \\ c_{2,3} &= -c_{3,2} = [10, 0, 0]^\top \\ c_{3,4} &= -c_{4,3} = [10, -10, 0]^\top \\ c_{4,5} &= -c_{5,4} = [-10, -10, 0]^\top \\ c_{1,0} &= [10, 10, 0]^\top \\ c_{3,0} &= [0, -10, 0]^\top \\ c_{5,0} &= [10, 10, 0]^\top \end{aligned}$$

For the third area, we set the regions of interest at $[50, -50, 10]^\top$, $[40, -40, 10]^\top$, $[60, -40, 10]^\top$, $[60, -50, 10]^\top$, $[40, -60, 10]^\top$, $[40, -50, 10]^\top$, and the desired formation offsets as

$$\begin{aligned} c_{1,2} &= -c_{2,1} = [20, 0, 0]^\top \\ c_{2,3} &= -c_{3,2} = [0, -10, 0]^\top \\ c_{3,4} &= -c_{4,3} = [-20, -10, 0]^\top \\ c_{4,5} &= -c_{5,4} = [0, 10, 0]^\top \\ c_{1,0} &= [10, -10, 0]^\top \\ c_{3,0} &= [-10, 0, 0]^\top \\ c_{5,0} &= [10, 0, 0]^\top \end{aligned}$$

The task formation instance as well as each formation instances for the generation of the trajectories for the training of the neural networks are created by assigning to the constants $m_i, A_{i,\ell}, \eta_{i,\ell}, \phi_{i,\ell}$ and the elements of F_i a random value in $(0, 1)$, and an initial agent condition for each agent as $x_{i,1}(0) = x_{0,1}(0) + \text{rand}(-10, 10)\bar{1}_3$, $x_{i,2}(0) = \text{rand}(-2, 2)\bar{1}_3$. The formation offsets and communication graph $\bar{\mathcal{G}}$ are the same in all cases (as specified above and in the

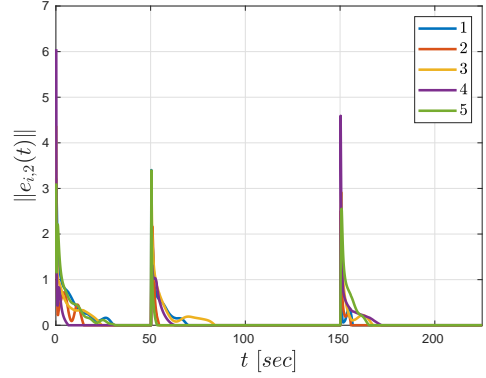


Figure 9: The evolution of the error norms $\|e_{i,2}(t)\|$ for $i \in \{1, \dots, 5\}$, and the second numerical experiment.

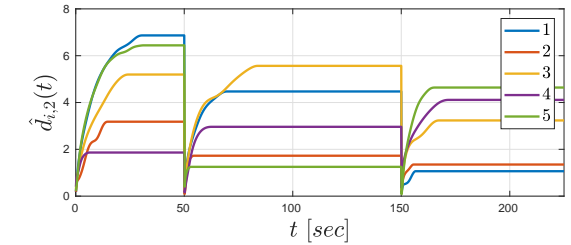
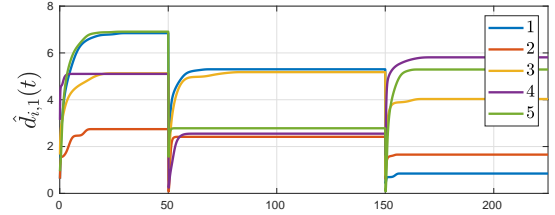


Figure 10: The evolution of the adaptation signals $\hat{d}_{i,1}(t)$ and $\hat{d}_{i,2}(t)$ for $i \in \{1, \dots, 5\}$, and the second numerical experiment.

main manuscript, respectively). The initial condition of the leader is always taken as $x_{0,1}(0) = [0, 0, 10]^\top$, $x_{0,2}(0) = [0, 0, 0]^\top$. The trajectory of the leader in the x - y plane is depicted in Fig. 3 of the main manuscript, whereas it increases linearly from 0 to 10 meters along the vertical z direction in the time interval $[0, 50]$ seconds, and remains there thereafter. The total duration of the task is 225 seconds. Similarly to the first experiment, more results are given in Figs. 9-11; Fig. 9 depicts the error norms $\|e_{i,2}(t)\|$, Fig. 10 depicts the adaptation signals $\hat{d}_{i,1}(t)$, $\hat{d}_{i,2}(t)$, and Fig. 11 depicts the control inputs u_i of the agents, as well as the respective outputs $u_{i,nn}$ of the neural networks, for $i \in \{1, \dots, 5\}$.

Case 3:

For the third experiment, we create 120 different formation instances $\mathcal{F}^k := (x_0^k, \bar{f}^k, \bar{g}^k, \bar{c}^k, \mathcal{G}^k, \bar{x}^k(0))$. In every instance k , we set the parameters in \bar{f}^k , and \bar{g}^k as in the previous cases, we set

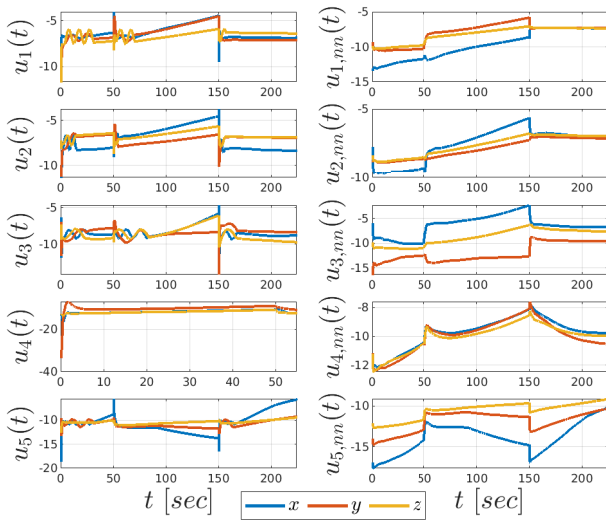


Figure 11: The evolution of the control inputs $u_i(t)$ (left) and the neural-network controllers $u_{i,nn}(t)$ (right), for $i \in \{1, \dots, 5\}$, and the second numerical experiment.

randomly the communication graph \mathcal{G}^k such that it satisfies Assumption 2, we set random offsets c_{ij} in the interval $(-5, 5)\mathbb{I}_3$, for $(i, j) \in \mathcal{E}$, and the initial conditions of the agents as $x_{i,1}(0) = \text{rand}(-10, 10)\mathbb{I}_3$, $x_{i,2}(0) = \text{rand}(-2.5, 2.5)\mathbb{I}_3$, for all $i \in \{1, \dots, 5\}$. Finally, the leader trajectory x_0 is set for each instance $k \in \{1, \dots, 120\}$ as follows: we create four points in \mathbb{R}^3 randomly in $(-10, 10)$ in the x - and y -directions, and in $(1, 20)$ in the z direction. We then create a random sequence of these points, and set the leader trajectory as a smooth path that visits them according to that sequence, with a duration of 40 seconds.